Substrate temperature and ion kinetic energy effects on first steps of He + implantation in tungsten: experiments and simulations

Lucile Pentecoste, Anne-Lise Thomann, Pascal Brault, Thomas Lecas, Pierre Desgardin, Thierry Sauvage, Marie-France Barthe

Substrate temperature and ion kinetic energy effects on first steps of He^+ implantation in tungsten: experiments and simulations

Lucile Pentecoste[a], Anne-Lise Thomann[a], Pascal Brault[a], Thomas Lecas[a], Pierre Desgardin[b], Thierry Sauvage[b], Marie-France Barthe[b]

[a] GREMI, CNRS/Université d'Orléans, 14 rue d'Issoudun, B.P. 6744, 45067 Orléans Cedex 2, France, [b] CNRS, UPR3079 CEMHTI, 1D avenue de la Recherche Scientifique, 45071 Orléans Cedex 2, France

Abstract:

Helium implantations are experimentally performed in order to observe the formation of vacancy defects in tungsten crystals. Characterizations with nuclear reaction analysis (NRA) and positron annihilation spectroscopy (DB-PAS) allow respectively to quantify the ^3He retention and to determine the nature of the vacancy defects formed during the process. Two types of defects are observed as a function of the impinging fluence: vacancies filled with He (He_nV and $He_nV_{m>1}$) below $2.5x10^{20}$ $He.m^{-2}$ and small voids above. The influence of kinetic energy of the impinging He atoms and of the substrate temperature during the implantation is studied. Molecular dynamic simulations of the implantations are performed to further understand the formation mechanisms of the initial He_nV defects. A good agreement is found between results obtained by simulation and experimentally. The implantation depth of the He atoms and the mobilities of He and W are identified as the main features governing the vacancy formation.

Keywords: Tungsten; Helium; Implantation/Irradiation; Molecular dynamics simulations; Vacancy generation

1. Introduction

In future fusion reactors, tungsten (W) used as a target of the divertor will be exposed to severe conditions: high heat loads and light particles bombardment [1,2]. Study of the W behavior when exposed to these fluxes is necessary to estimate the lifetime of these fusion reactor components. Experiments involving exposition of W surfaces to high fluxes and high fluences of helium (He) in dedicated reactors like NAGDIS and PISCES have been performed [3,4]. These studies showed that the W surface morphology is modified even for kinetic energies of impinging ions below the displacement threshold of W lattice atoms [5,6]. It has been shown that under corresponding ion fluxes, He/W interaction could lead to the formation of holes, blisters, fuzz etc. and finally to flaking [7–11]. These structures are thought to be the consequences of the initial formation of vacancies and point defects into the W lattice [12].

In our previous work the mechanisms involved in the defect formation due to the retention of He in the W lattice have been investigated through experiments and MD simulations [13]. It has been shown that for kinetic energy of 300 eV, above a fluence of 2.5×10^{20} $He.m^{-2}$, the amount of implanted He atoms saturates. This corresponds to the limit of the accumulation of He atoms within W vacancies (He-vacancy complexes) and the beginning of the formation of large He free voids in the W lattice due to the emptying of the large He clusters through the surface (or *cluster rupture* events). These voids extend to a few nanometers beneath the surface when He^+ implantation energy is 300 eV.

The present study aims to observe the influence of the He ion kinetic energy and of the W lattice temperature on the first steps of the vacancy-type defects formation in W crystal. The conditions are defined to only study the effect of He accumulation inside the W lattice. That means the kinetic energy of the He ions ranges from 100 to 500 eV, transferring a maximum of energy ranging from 8.33 to 41.65 eV through any elastic collisions with a W atom. Those values are below the displacement threshold of a W atom by an impinging He atom which equals 90 eV [5,6,14]. The W substrate temperature was set between 173 and 873 K. Implantations were performed both experimentally in a homemade ICP plasma source and by molecular dynamics simulations. Polycrystalline W samples were analyzed before and after implantation by means of nuclear reaction analysis (NRA) and positron annihilation spectroscopy (DB-PAS) to determine the He retention and to qualify the vacancy defects, respectively. Simulation data were treated to bring out the total calculated implanted fluence (retention), the He concentration profiles and to observe the formation of initials He_n-V clusters.

2. Experiments and model

2.1. Experimental conditions of implantations and material analysis techniques

2.1.1. Sample preparation and He implantation

Polycrystalline W samples are $7 \times 7 \times 0.3$ mm^3 pieces of 99.95% purity. The samples were prepared in order to remove at best the initial defects. The complete preparation procedure is detailed in reference [14]. After the preparation, the samples exhibit large size grains (hundreds of μm^2), minimizing the surface of grain boundaries.

A dedicated Radio-Frequency Inductively Coupled Plasma source was developed at GREMI to perform He implantations. For a complete description and characterization of the source please refer to [14]. The W substrates are placed in a reactor initially pumped down to 10^{-4} Pa. They are then exposed to He ions with a kinetic energy ranging from 100 to 500 eV depending on the DC bias voltage applied to the substrate holder (voltage supply: Midec SK 600V-0,5A max); the fluxes ranged from 10^{15} to 10^{18} He.m^{-2} s^{-1}. Typically in those conditions, kinetic energy of the ions is supposed to be equivalent to the difference between the plasma and the surface potentials (V_p-V_b), since the ions are accelerated from the plasma through the sheath forming at the surface of the substrate. In the present study, the plasma potential V_p is measured to range between +10 and +20 V and the surface bias V_b is set negatively to 100, 300 or 500 V depending on the implantation experiment. However, we have shown from measurements performed with an energy analyzer that the energy distribution function of the ions starts from the V_p-V_b values and that the FWHM can be relatively broad, depending on the discharge coupling regime [14]. This is not the scope of the present work to study the effect of the real distribution function. Hence to ease the reading in the following, the implantation conditions will be labelled with the maximum kinetic energy value, i.e. the potential applied to the substrate surfaces. Implantations were performed on samples maintained at temperatures ranging from 173 to 873 K. Samples were fixed on a temperature regulated substrate holder. A liquid nitrogen circulation was used to reach the lowest temperatures.

The impinging ion fluences were chosen to be below and above 2.5×10^{20} He.m^{-2}, fluence limit of the accumulation of He atoms within W vacancies (He-vacancy complexes) at an implantation energy of 300 eV [14,15]. The fluence is the total number of impinging ions for a given bombardment duration; it is calculated from the ion flux obtained from the measurement of the

ionic current at the substrate. ^{3}He isotope was chosen instead of ^{4}He because it can be quantified using the nuclear reaction analysis technique (NRA).

2.1.2. NRA measurements

The total amount of ^{3}He retained in the samples was measured by NRA in a dedicated apparatus DIADDHEM at the CEMHTI [16] laboratory, Orléans. The nuclear reaction used to quantify the He content is ^{3}He(d,^{1}H)α [17–20]. A 900 keV deuterium beam is used to induce the nuclear reaction with ^{3}He atoms present in the W substrate. The nuclear reaction products are a ^{4}He (α particle) and a ^{1}H (proton) with energies of 2-3 and 15 MeV, respectively. The concentration of retained ^{3}He is determined by counting the emitted protons for a given deuterium beam charge. The total proton number is normalized by the beam charge and compared to the one measured with the same analysis conditions in a standard sample containing 10^{20} ^{3}He.m^{-2}. The cross section of the ^{3}He(d,^{1}H)α nuclear reaction for 900 keV incident deuterons in W is quasi-constant (relative standard deviation of 5%) up to a depth of 300 nm. In regard to the low implantation depth of He ions (20 nm for 500 eV), the ^{3}He concentration is determined using a simple proportionality relation.

2.1.3. Positron Annihilation Spectroscopy

In order to qualify the vacancy defects present before and formed after the implantation process, the positron annihilation spectroscopy was used. This technique is based on the analysis of the Doppler broadening of the gamma ray emitted at 511 keV during the positron annihilation process (DB-PAS). The annihilation γ ray undergoes a Doppler broadening due to the various

kinetic momentum of annihilated electron-positron pairs. It is then possible to get an image of the kinetic momentum distribution of the electrons of the sample and thus to probe the electronic density encountered by the positron in the sample. Also, when implanted into the sample and due to their positive charge, positrons are preferentially trapped by vacancy-type defects. Thus the technique is particularly sensitive to the nature and concentration of vacancy defects in the sample. More details on DB-PAS could be found in [15,21].

At the CEMHTI laboratory, the DB-PAS is implemented with a slow positron beam which enables to implant monoenergetic positrons in the samples with variable energy E ranging from 300 eV to 25 keV [22]. It allows probing the annihilation characteristics of the sample as a function of the depth from 0.4 to 700 nm [23]. The positron-electron pair momentum distribution is measured at 300 K by recording the Doppler broadening of the 511-keV annihilation line with a Ge detector. A spectrum of approximately 10^6 events is collected at each positron energy value. In order to follow the evolution of the annihilation peak as the function of the positron energy, two shape parameters are extracted from the spectrum. The low momentum parameter S is the fraction of annihilations taking place in the low momentum range i.e. a window close to 511 keV and corresponds to annihilation with valance electrons. The high-momentum parameter W_p in the windows at the wings, corresponds to the fraction of annihilations taking place with core electrons in the momentum range close to 506 and 516 keV [21].

It is important to note that each annihilation states (i.e. defect, bulk, surface…) is characterized with specific S and W_p values and when a material contains vacancy defects S increases and W_p decreases. However, in the case of He implantation in matter, a decrease of the S parameter and an increase of the W_p parameter could be observed [24,25]. It is linked to the filling of the vacancies, also called decoration of the vacancies, by the He atoms that change the electron

momentum distribution into defects. As W_p parameter always behaves in the opposite way of S parameter, we will only present S(E) curves in this paper.

Also, most of our interpretations of DB-PAS data are made from the analysis of the evolution of the S parameter from the initial state of the prepared sample to its implanted state. To clarify some evolutions and to quantify the difference between the initial and the implanted states, $\Delta S/S$ parameter will be used. It is defined as the relative difference between the mean values of S $(S_{final}-S_{initial})/S_{initial})$ in the positron kinetic energy range of 2 keV - 4 keV, corresponding to the near surface of W (up to 35 nm thickness) where He implantation is expected to take place.

The positronium fraction (Ps) can also be used as a proof of the presence of defects into the sample. In case of dense metals, Ps is formed with backscattered or reemitted positrons from the surface and a free electron. It is furthered when positrons are not efficiently trapped inside the sample and are thus able to diffuse back to the surface. The fraction of emitted positronium is consequently a kind of signature of the trapping rate of positrons inside the material, which is related to the concentration of defects. As an example, the positronium fraction evolution with the positron energy is given in figure 1 for a W sample before and after preparation. Below 2 keV, surface acts as a strong positron trap and very low energy positrons can easily diffuse back and be reemitted to form positronium, hence the high values in this range are not interpreted. Between 2 and 10 keV, the positronium fraction is low in the as received sample whereas it is still high in the prepared sample. This high value indicates that the number of trapping sites (i.e. vacancy defects) is low, and thus that the preparation procedure was efficient to remove initial vacancy defects.

In this work the parameter ΔPs/Ps, defined as the mean value in the energy range 2 to 4 keV of the ratio $(Ps_{final}-Ps_{initial})/Ps_{initial}$ will be calculated to evaluate the magnitude of the modification between initial and implanted states.

2.2. Molecular dynamic simulation model

To investigate the phenomena occurring during the implantation of He into W, molecular dynamic simulations are carried out on an Alineos quadriprocessor 8 cores high performance computer using LAMMPS [26]. Complete description of the model and of the data treatment could be found in reference [13], we only give here the most important points of the simulation.

A (100) body-centered cubic W crystal box consisting of 17 × 17 × 204 unit cells is built, for which dimensions are then 53.8 × 53.8 × 645.7 Å. Periodic boundaries conditions are set in the x [100] and y [010] directions, and free motion is allowed along z [001] to figure the surface of a monocrystal. The bottom of the box is composed of a fixed layer of 6 unit cells (20.5 Å) which mimics the unperturbed bulk. The speed of the remaining W atoms is selected randomly from a Maxwell-Boltzmann distribution corresponding to the thermal energy at the investigated temperature which is maintained thanks to a Berendsen thermostat [27]. The thermostat is used because the fluxes of impinging atoms used in MD simulations are unphysically high as compared to the experiments. High fluxes are used in order to reduce the calculation durations taking properly into account He interactions with W and with He already present in W [13]. Substrate thickness is chosen in order to limit to 0.5% the implanted He atoms crossing the substrate through the fixed W atom bottom layers.

He ions are treated as atoms, as they are neutralized at the W surface, so classical MD simulations are applicable. He atoms are injected one by one and in a direction normal to the surface. They carry a fixed kinetic energy corresponding to the mean value expected in the experiments. The frequency of the He atom injection is set to 5 $He.ps^{-1}$. Such impingement frequency allows no lateral interaction between induced perturbations in the W crystal during the dissipation time, due to the large enough substrate width. The lattice displacement threshold for a W atom is of 90 eV, and the maximum energy transferred E_{tr} from a He atom to a W atom is obtained from the elastic collision energy transfer formula: $E_{tr} / E_i = 4m_1m_2/ (m_1+m_2)^2$ [28] it ranges from 1.66 to 41.65 eV for incident energies ranging from 20 to 500 eV. The number of He atoms impinging the W surface ranges from 2000 to 10000 for a surface of 53.8×53.8 $Å^2$. This corresponds to the fluences ranging from 10^{18} to 10^{21} $He.m^{-2}$.

Handling molecular dynamics requires the knowledge of inter-atomic potentials and a set of initial conditions. We use the Juslin and Wirth potentials [29]: W-W interactions are described by a modified Ackland-Therford potential and W-He interactions are modelled from DFT study. Finally, He-He interactions in the substrate are described by Beck's potential [30], which allows He cluster growth. Implantation conditions were chosen to match at the best with experiments: the temperature of the W simulation box was varied between 173 and 873 K and the incident He atom kinetic energy between 100 and 500 eV at normal incidence.

The data extracted from the simulations are frames presenting the successive positions of each atoms (He and W) every 2 ps, i.e. after each the injection of 10 He atoms in the simulation box. Those are treated with the VMD software [31] which allows observation of the trajectories and the measurements of radial distribution functions of the atoms (RDF). Also a home-made

program especially written to count the number of He clusters and determine their content of He over the successive frames or time steps.

3. Results and discussion

3.1. Detailed study of the formation of He-vacancy complexes

The initial He_n-V clusters are studied from a statistical point of view. The He_n clusters are groups of He atoms defined by an interatomic distance low compared to the W crystal lattice parameter (a = 3.1652 Å). These clusters form as soon as two He atoms meet in the W lattice and migrate together until being reached by new He atoms. At some point, the cluster formed stops migrating into the lattice since its volume does not allow interstitial movements between the W atoms anymore. The mean distance (rc) between the aggregated He_n atoms is determined from the radial distribution function (RDF). The figure 2 presents the various RDFs obtained in each conditions of kinetic energies (from 20 to 500 eV) and temperatures (from 173 to 873 K) at the end of the simulations.

The RDF curves present a distribution ranging from 1 to 5 Å. In each case a maximum is observed for a distance rc of 1.75 Å. However, the distribution of interatomic He-He distances indicates that some atoms can be further away from each other within a distance of 5 Å. Either those He atoms are second neighbors or the thermal agitation induces a wider distribution of the distances between He. Hence, in order to calculate the number of clusters and the number of He they contains, multiples of the distance are defined as rc. 4 various calculations are performed with 1, 1.5, 2 and 3*rc. The histograms obtained for each frames in the case of 20 eV and 300 K implantation is presented in figure 3.

These histograms allow following the growth of He_n clusters along the simulation as the number of implanted He atoms increases. From the intensity of the color scale obtained in each histogram, the optimum rc value to use can be determined in order to get the most information as possible from the calculations. Indeed, if rc is limited to 1.75 Å, clusters with He atoms parting due to the thermal agitation are not considered and statistically absent from the clusters, even if they are actually present in the simulated lattice. Therefore, the histograms compared for the various implantation conditions are the ones calculated with a value of 1.5*rc, which includes most of the first neighbors without overlapping to many clusters.

Limiting the study to the first 200 frames shows the formation of the primary He_n clusters. The figure 4 presents the histogram for the case simulated with He kinetic energy set at 300 eV and W substrate temperature set at 300 K. This histogram presents a leveling which corresponds to the formation of clusters containing 7 He atoms. The trajectories of He atoms contained in such clusters observed with the visualization software shows that they are immobile in the lattice. The He_7 clusters do not have the possibility to move and pushes a W atom away from its lattice location. This information is correlated to the "self-trapping" i.e. the formation of a Frenkel pair (a vacancy and a self-interstitial), $He_7 \rightarrow He_7\text{-}V + I$ with V being a W vacancy and I a self-interstitial of W (SIA) [32,33]. Below this number, the $He_{n<7}$ clusters are mobile in the lattice and migrate interstitially. Above this number, $He_{n>7}$ clusters are considered as larger complexes or bubbles (He_nV_m) which form through trap mutation, i.e. the insertion of He atoms into a large clusters surpressurizing it and leading to the formation of a new vacancy and a new W interstitial ($He_nV_m + He \rightarrow He_{n+1}V_{m+1} + I$).

From the histogram, it is also possible to follow the growth of a cluster by observing the main lines of the graph as a function of the frame, such as pointed out by the blue arrows on the figure

4. Indeed, the speed of growth could be determined for the main clusters. However these rates are not constant over time since the growth takes place along different ways. The lowest speed rates corresponds to the addition of singles He atoms to the clusters while the highest speed rates, i.e. arrows with high slope, are due to the merging of clusters containing a large number of He. The disappearance of clusters of a high number of He is then due to either their merging with another cluster or, in the case of low energy implantations (20 and 100 eV), to their desorption from the substrate as will be described in the next section.

The number of He necessary to form a Frenkel pair is given for each implantation conditions in the tables 1.a and b. For the He kinetic energy influence study, the W substrate temperature is fixed at 300 K, and for the W substrate temperature influence study, the incident kinetic energy of the He is fixed at 300 eV.

For each simulations, the number of He necessary to form a Frenkel pair is roughly equivalent. Note that for the 300 eV / 873 K case, the determination of the number of He was not possible due to the absence of plateau and the low number of clusters over the simulation before the rupture of the substrate due to a single massive cluster close to the surface.

In those simulations, the formation of Frenkel pairs is not influenced by the kinetic energy of the incident He. Indeed, in this range of energies, the accumulation is the only way He can induce the displacement of W atoms in the lattice. However, one could expect a newly implanted He atoms depositing its kinetic energy directly in a cluster could bring enough energy to form a vacancy. In this series of simulations, such event was not observed and was not evidenced statistically. In the case of the substrate temperature influence study, the same results are obtained. The increased mobility of the W atoms does not influence the formation of the initial Frenkel pairs for the temperatures ranging from 173 to 873 K.

As soon as the initial He_nV complex is formed, the lattice reorganizes itself in order to place the SIA of W in a lattice position. The SIA is typically ejected along the (111) direction since the potential used for these simulations proposes the lowest energy (9.55 eV) for this type of displacement [29]. Subsequently the whole row of W atoms are pushed to reorganize the lattice along the (111) direction toward energy "sinks" i.e. the surface or an already formed bubbles. The movement of the W atoms along the 111 row are called "loop-punching". Those events have been evidenced in MD simulations by many authors [34–36] and are favored by the potentials used for these MD simulations.

The "loop-punching" events were observed individually on the simulated implantations performed at energies ranging from 20 to 500 eV at 300 K and the ones performed at temperatures ranging from 173 to 300 K with an incident kinetic energy of the He ions of 300 eV. On the one hand, the kinetic energy of the incident He atoms has not shown any influence on these displacements in the range of energies used for those simulations. On the other hand, the study of the substrate temperature influence has not shown any influence on this type of defect formation between 173 and 300 K. However, for the simulations of implantation performed at higher temperature of substrates (473 to 873 K), a disorder is rapidly generated in the W layers close to the surface as shown on the snapshots of the figure 12.a. For these higher temperatures, this disorder does not allow anymore the observation of the W movements along any crystalline direction. Hence no conclusion on the influence of the substrate temperature on the mechanisms of "loop-punching" are drawn from the simulations performed at temperatures ranging from 473 to 873 K.

3.2. Comparisons of experimental and simulation results

3.2.1. Characteristics of He implantation in W at kinetic energy of 300 eV

Such as described in the previous paragraphs and in our previous work, the course of a typical implantation run has been followed for 300 eV He atom kinetic energy and a W substrate temperature of 300 K by MD simulations [13]. Three steps have been evidenced when the number of implanted He atoms increases inside the W lattice:

- He penetrates the substrate and diffuses interstitially, until it encounters another He atom.

- Two He atoms form a cluster which becomes a trap site for other incoming He atoms. When the number of aggregated He atoms exceeds 6, the cluster stops migrating and form a He_nV cluster such as was described in the previous paragraphs. The stratification observed on the calculated depth profiles is due to the formation of clusters at different depths which prevents the migration deeper in the thickness.

- Formed He_nV clusters grow and coalesce into He_nV_m complexes beneath W substrate surface until He concentration becomes high enough to lead to W flaking.

Very good agreement was found between experiments and MD simulations, and a saturation of the number of He atoms incorporated inside the W substrate was evidenced by both approaches. This saturation phenomenon of the retention rate occurs at an impinging atom number of 2×10^{20} $He.m^{-2}$; the maximum reached He retention being 5×10^{19} $He.m^{-2}$. This behavior was explained by the release of He atoms by cluster rupture and diffusion towards the surface [13].

The evolution of the S DB-PAS parameter as function of the positron kinetic energy is given in figure 5. In the kinetic range 2 to 5 keV, a clear change in the S behavior is observed. Below an impinging fluence of 10^{21} $He.m^{-2}$, the S parameter is lower than the value measured on the non-implanted sample, whereas it becomes higher after 2.5×10^{21} $He.m^{-2}$. The corresponding $\Delta S/S$

parameter evolution with respect to the impinging fluence is presented together with the He retention obtained by NRA in figure 6.

During the linear increase of the retention, before the saturation step, the ΔS/S ratio remains negative. As mentioned before, a negative ΔS/S value is specific of He insertion in vacancy defects. It is characteristic of the filling of the W vacancies by He [15,24,25]. Thus the observed evolution with increasing fluence below the saturation step indicates that accumulation of He inside the W lattice induces the displacement of W atoms to form vacancies where He is trapped. The involved mechanism is the self trapping and the trap mutation described in the previous section.

When the saturation point is reached, the ΔS/S ratio becomes positive revealing the presence of large free volumes. This behavior means that after the filling of first formed W vacancies (He_nV and He_nV_m), when the He fluence increases, larger He_nV_m complexes are formed, through further loop punching and trap mutation events, those are able to reach the surface and empty themselves through it leaving voids into the W lattice.

The trends obtained by measurements and MD simulations are similar. A retention saturation is reached above 2×10^{20} $He.m^{-2}$. Below this fluence, W vacancies are created and progressively filled by incoming He atoms; above there is a clear modification in the He insertion regime: larger free volumes are present and the accumulation of He at the near W surface (because of the low kinetic energy of He ions) seems to lead to the release of He through the surface (by flaking) which causes the saturation of He retention. To go further into the understanding of such behaviors, numerical and experimental implantations have been performed by varying parameters

expected to drive the implantation process: kinetic energy of the incoming ions and W substrate temperature.

3.2.2. Helium ion kinetic energy effect

Implantations were carried out at three kinetic energies below or close to the displacement threshold of W by He ions, which is around 500 eV, in order to investigate the effect of He accumulation.

From the snapshots illustrating He implanted into W at a retention of 1.3×10^{19} $He.m^{-2}$ for various kinetic energies shown in figure 7.a, and the corresponding concentration profiles (figure 7.b), it is clearly seen that He atoms are able to diffuse deeper when the kinetic energy rises. This is easily understandable and has already been reported [37–39]. For 20 eV and 100 eV the diffusion depth is similar, of the order of 5 nm, and it reaches 20 nm at 500 eV. Dispersion of implanted He over a larger depth, of course, promotes the retention inside the W.

He atoms being dispersed over a shallower depth at low kinetic energies (see the narrow profiles of figure 7.b as compared to high energies), the size of He clusters is larger. At 20 eV and 100 eV, bubbles are clearly present very close to the surface. The pressure inside these bubbles could become very high and lead to local rupture of the superficial W layer. This mechanisms of cluster rupture is observed for both kinetic energies and causes the release of He from the W lattice [34,40,41].

To evidence such mechanisms, the retention rate has been plotted versus calculation time, i.e. for increasing impinging He atom number (figure 8).

At 20 eV and 100 eV numerous abrupt falls are observed on the curves. They are due to successive cluster emptying events. Hence after the local release of He, another cluster grows in size and reaches the critical He amount or/and pressure to break. This phenomenon limits the total incorporation of He and is clearly the cause of the saturation behavior of the fluence. At 300 eV, a single rupture is observed. Because implantation takes place in a larger depth, the retention required for a cluster to contain sufficient He amount to break is higher. If the implantation had lasted longer another rupture would have most probably occurred. For 500 eV, the retention rate remains constant, indicating that the critical (or saturation fluence) is not reached yet.

Results of NRA analysis are given in figure 9.a for an incoming fluence at (2.5×10^{20} He.m^{-2}) and above (3.1×10^{21} He.m^{-2}) the saturation step for 300 eV ions. The retentions calculated from MD data are also plotted, those values correspond to the maximum He retention obtained for the highest simulated impinging fluences which are 6.9×10^{19} He.m^{-2} for the 20 eV simulation and 2.05×10^{20} He.m^{-2} for the other kinetic energies. For the simulation performed at a kinetic energy of 300 eV, the retention reported value corresponds to the state before the substrate rupture that means at the saturation impinging fluence which is 1.57×10^{20} He.m^{-2}. Corresponding snapshots are presented in figure 9.b.

The results in figure 9.a show that the experimental retention is lower than the simulated one. The difference is mainly attributed to the release of non-trapped He from the samples. Indeed, MD gives the number of implanted He atoms at the end of the implantation process but does not take into account possible evolution after implantation. He is well known to be very mobile in W even at room temperature [42,43] and it is highly probable that interstitial isolated He atoms and small clusters are able to migrate and reach the substrate surface to escape. In other words MD

simulations give the total number of implanted He atoms and NRA the number of retained He atoms, that means efficiently trapped inside the W lattice.

However, in figure 9 the trends obtained from both experiments and simulation are in very good agreement: the retention rises when the kinetic energy increases. The value obtained for the highest incident fluence at 500 eV lies above the maximum retention found at 300 eV (5×10^{19} $He.m^{-2}$), showing that the retention at saturation is different depending on the kinetic energy.

DB-PAS results (S(E) evolution and $\Delta S/S$ as function of the kinetic energy of He) are given in figure 10 for two fluences 2.5×10^{20} $He.m^{-2}$ and 3.1×10^{21} $He.m^{-2}$.

At low fluence, whatever the kinetic energy, the S parameter of the implanted state is lower than that of the initial one (negative $\Delta S/S$ ratio). However the low positronium emission fraction found for positron energies ranging from 2 keV to 4 keV ($\Delta Ps/Ps$ around -0.95 for all He kinetic energies) indicates that positrons are efficiently trapped into the defects. Hence vacancies are generated during the implantation whatever the incident He ions kinetic energy. Again, this proves that W vacancies are formed by "self trapping" and filled by He which leads to a decrease of the S parameter. The S(E) and $\Delta S/S$, $\Delta Ps/Ps$ ratios are similar for all the kinetic energies, that means no difference between implanted states are detected by DB-PAS.

At high fluence, differences are observed depending on the kinetic energy. The S parameter is higher than that at low fluence and increases with the energy. The $\Delta S/S$ ratio increases with the kinetic energy and becomes positive above 100 eV. From all these trends it can be deduced that larger free voids or larger He_nV_m complexes are detected at highest He implantation energies.

All these DB-PAS results could appear in contradiction with MD results that suggest a large difference of defect size (large clusters and, thus, large W vacancies) and in-depth distribution

depending on the energy. Formation of extended defects is promoted close to the surface at low kinetic energies, whereas, smaller defects are formed deeper in the depth at kinetic energies higher than 100 eV (see figure 7.a).

However, one has to keep in mind that area below 5 nm is difficult to probe by DB-PAS because the vicinity of the surface influences the data. As mentioned above, positrons with energy below 2 keV can easily diffuse back to the surface and be reemitted leading to positronium emission. This effect prevents positron trapping into defects and the positronium decay can have an influence on the S measured value. Clearly at 20 and 100 eV, the defects present in the depth where the implantation mainly takes place may not be efficiently probed by DB-PAS and only the zone deeper than the He implanted profile is analyzed. The main features of the implanted sample thus becomes not detectable at low kinetic energies.

This could explain the fact that similar implanted states are detected at low fluence whatever the kinetic energy, and the following conclusions can be made: 1) He filled vacancies are formed in the main part of the implanted zone; 2) MD seems to underestimate He diffusion inside the W lattice since those defects are detected by DB-PAS well below the predicted He implanted depth at low kinetic energies.

For higher fluences, the He atoms accumulate in a very limited depth at low kinetic energy leading to the formation of larger vacancy defects close to the surface which furthers He escape from the surface and thus limits the retention at saturation. This limited He insertion at low energy associated to the formation of large defects deeper in the thickness at high energy, leads to the profiles presented in figure 7.b for a retention of 1.3×10^{19} He.m^{-2}. It is clearly visible on the presented snapshots of figure 7.a and 9.b, that over the depth (5 to 20 nm) correctly probed by positrons, larger vacancy defects are present when incident He have a kinetic energy of 500 eV

rather than 300 eV : this is in agreement with DB-PAS results. Further comparison between experiments and simulations may not be relevant because, as shown on the graph of figure 9.a, the retention values are much higher in the simulations than experimentally. However trends deduced from the snapshots remain valid.

Thus both experiments and simulations give the following trends for implantations performed for increasing kinetic energies: 1) for a given impinging fluence the retention of He is promoted; 2) He is implanted deeper, consequently the accumulation taking place on an extended area and thus the rupture of the W surface is delayed; 3) despite the slower vacancy formation rate, He_nV complexes are formed even at low fluences. Those He filled vacancies are certainly more distributed over the depth than for the low kinetic energy implantations; 4) At high fluences, larger He-vacancies complexes are formed through trap mutations occurring deeper than at low incident kinetic energies.

3.2.3. Substrate temperature effect

Experiments and MD simulations were performed at 173, 300, 473, 673 and 873 K for a kinetic energy of He ions of 300 eV. The measured and calculated retention levels are presented in figure 11 for a high and a low impinging fluence.

Evolutions evidenced in experiments and simulations are in good agreement and exhibit a decrease of the retention fluence when the substrate temperature increases. Experimentally, the measured retention fluence at 173 K deviates from the general trends. We attribute this phenomenon to the presence at low temperature of a contamination layer on the reactor and substrate holder surfaces that can prevent He ions from penetrating the lattice and limits the

formation of the defects. This contaminant layer is due to the presence of water vapor in the reactor initially pumped down to 10^{-4} Pa.

ΔS/S and ΔPs/Ps ratios are plotted in figure 11 as a function of the substrate temperature.

First at high impinging fluence (figure 11.b), the constant and very low value of ΔPs/Ps indicates that efficient trapping of the positron into defects occurs at all the temperatures, i.e. defects have been generated. The ΔS/S ratio is found to decrease from positive to negative value as the temperature increases. This is associated to a decrease of the He retention, indicating that the number and/or size of the vacancy defects diminishes with the temperature. The type of defects is also affected by the temperature: at high temperature He filled vacancies are mainly formed, while larger free voids are detected at low temperatures. This is in contradiction with the literature since the rise of the temperature leads in general to the formation of larger He-vacancy complexes due to the increased mobility of such defects which merge together [44,45]. This point will be discussed in the next paragraphs.

At low impinging fluence ΔS/S values are negative, thus the main detected defects are vacancies filled with He, as already evidenced in the study of the kinetic energy influence. Except for the 173 K sample, a clear increase of the ΔPs/Ps ratio is observed when the temperature rises. This proves that the positron trapping efficiency varies i.e. the defect formation depends on the temperature of the W substrate. It is the opposite of what has been obtained at high impinging fluence: the quantity of defects formed decreases when the temperature rises. Since the He retention decreases, this behavior evidences the difficulty of He to be trapped in a heated W lattice. Indeed the increased mobility of the formed point defects such as SIA or vacancies at higher temperature can lead to their migration toward sinks e.g. surface or grain boundaries

[46,47], hence instead of merging and growing in size, most of them are lost to the substrate surface [44,45]. In other words, the thermal motion of W atoms hinders the He trapping process while enhancing the motion of the He-vacancies defects toward the surface.

In the following, observations made above will be compared to results of MD simulations performed at 300 eV. To study He accumulation versus lattice temperature, snapshots and He concentration profiles are displayed in figure 13 for the same retention of 1.4×10^{19} He.m^{-2}. As compared to the evolution with the kinetic energy, He implanted profiles appear much less affected by the lattice temperature. Indeed, implanted He atoms lie below the first 20 nm in all cases. However, an accurate observation of the He profiles shows that He atoms remain closer to the surface when the temperature is increased. Indeed, the main peak extends to 10 nm depth for 173 and 273 K, whereas it is limited to the first 5 nm for 673 and 873 K. Thus the general trend is that the thermal excitation hinders the migration of He far from the surface.

The clearest effect evidenced by MD snapshots is that the W superficial layer is widely affected by He implantation at highest temperatures: it becomes amorphous. This is unexpected at such low temperature since experimentally the melting point of W is 3695 K and for a MD simulation with the potentials used it should correspond to 4100 ± 50 K [29]. Simulations of W maintained at high temperatures and 873 K without impinging He, did not show amorphization of the top layers of the model substrate. This means, this disordered layer at the W surface only appears when He implantation takes place. This can show that W atoms are able to leave their lattice sites more easily at high temperature and that defects induced by He implantation and accumulation certainly become mobile. It is well known that vacancies and all defects migrations are furthered with temperature that will induce large vacancy clusters formation [44,45,48]. However, their mobility is increased toward the surface where they are lost. For instance, experimentally, Lee et

al. [49], whose irradiations of W with He are performed at low energy (500 eV) such as in the present study, determine from thermal desorption spectrometry (TDS) that at 500 K low energy bounded He clusters at grain boundaries or in the lattice close to dislocation loops desorbs.
Our PAS and NRA results indicate that, at low fluences, the reorganization phenomenon leads to the reduction of the number of defects that are exclusively He filled mono-vacancies due to the loss at the surface of the large defects. These results are then well described by our MD simulation data, which tend to validate the use of this model for He implantation in W. On snapshots corresponding to 4×10^{19} He.m^{-2} incoming fluence (figure 12.a), it is seen that, over the DB-PAS analysis depth, the number of implanted He and formed cluster defects is slightly lower at high temperature.

At high fluences the number of free voids decreases evidencing the loss of the large defects to the surface. Again the trend observed on corresponding MD snapshots in figure 12.b is similar. In the DB-PAS analyzed area the number and size of He clusters decrease as the temperature rises. The mobility of defects induces the formation of large He_nV_m clusters close enough to the surface to provoke “cluster rupture” events (as observed in the simulations at 473 K) or substrate rupture as observed in the simulations performed at 673 and 873 K, such as in the case of the low kinetic energies implantation simulations (20 and 100 eV). He clusters are emptied through the surface and escape, which makes the saturation occur earlier and explains the decrease of the retained He atom number measured by NRA and predicted by MD as the temperature rises.

4. Conclusion

We have shown in this work that the correlation between characterizations of experimentally implanted W samples and MD simulations of the implantation process leads to a better understanding of the involved elementary mechanisms. DB-PAS and NRA analyses have been carried out in order to evidence vacancy defect formation and to quantify the amount of He retained inside the lattice, respectively. From MD simulation data treatment it is possible to calculate the total amount of implanted He at the end of the implantation process, the He concentration profiles, and the size of the formed He clusters or bubbles at the beginning of the implantation, which are related to the presence of W lattice defects. It is also possible to determine the elementary processes occurring at the atomic level like He diffusion and aggregation, W lattice displacements and defect creation like He_nV complexes and loop punching.

A possible limitation of MD is that the implantation process is assumed to take place in a monocrystal of W. Nevertheless this assumption is not far from the reality of the low kinetic energy He/W interaction case. Indeed, He being very mobile in W and being implanted at the very near surface, an implanted atom has little chance to reach a grain boundary. Experimentally, in the used W polycrystalline samples, the grains measure typically several hundreds of square micrometers. Thus grain boundaries are not expected to play an important role on the implantation and retention processes, all grains acting as an isolated single crystal. This fact could be the reason for the good agreement found in the present work between simulation predictions and experimental results.

Study depending on the kinetic energy of the impinging ions (in the range 20 to 500 eV, below or close to the W displacement threshold by He ions) has shown that He diffuses deeply inside the W thickness as the energy is increased. Consequently, less He atoms are able to migrate toward

the surface and escape, which leads to a higher amount of trapped He in large clusters. Moreover, as dispersion of the implanted He takes place over a larger depth, the saturation step is thus delayed.

An increase of the W temperature during the implantation process, in the investigated range (173 to 873 K), has been shown to only weakly influence the He concentration profiles. However the thermal excitation of the W lattice impedes the formation and the stability of defects and furthers their loss to the surface so that less clusters or smaller ones are obtained.

It has been proved in this work that the initial repartition and further mobility of He atoms inside the W lattice are the driving parameters of the number and of the kind of formed defects, in this particular implantation regime for which no defects are able to be created by He ion direct impact.

Acknowledgements:

The Région Centre Val de Loire and CNRS are acknowledged for the financial support of this study.

References

[1] A.W. Kleyn, W. Koppers, N. Lopes Cardozo, Plasma-surface interaction in ITER, Vacuum. 80 (2006) 1098–1106. doi:10.1016/j.vacuum.2006.02.019.

[2] R.E. Nygren, R. Raffray, D. Whyte, M. a. Urickson, M. Baldwin, L.L. Snead, Making tungsten work - ICFRM-14 session T26 paper 501 Nygren et al. making tungsten work, J. Nucl. Mater. 417 (2011) 451–456. doi:10.1016/j.jnucmat.2010.12.289.

[3] D.M. Goebel, G. Campbell, R.W. Conn, Plasma surface interaction experimental facility (PISCES) for materials and edge physics studies, J. Nucl. Mater. 121 (1984) 277–282.

[4] S. Kajita, N. Ohno, M. Yajima, J. Kato, Growth annealing equilibrium of tungsten

nanostructures by helium plasma irradiation in non-eroding regimes, J. Nucl. Mater. 440 (2013) 55–62. doi:10.1016/j.jnucmat.2013.04.040.

[5] F. Maury, M. Biget, P. Vajda, A. Lucasson, P. Lucasson, Frenkel pair creation and stage I recovery in W crystals irradiated near threshold, Radiat. Eff. 38 (1978) 53–65.

[6] ASTM E521-9, Standard Practice for Neutron Radiation Damage Simulation by Charge-Particle Irradiation, in: Annu. B. ASTM Stand., American Society for Testing and Materials, Philadelphia, 1996: p. 1.

[7] D. Nishijima, M.Y. Ye, N. Ohno, S. Takamura, Formation mechanism of bubbles and holes on tungsten surface with low-energy and high-flux helium plasma irradiation in NAGDIS-II, J. Nucl. Mater. 329–333 (2004) 1029–1033. doi:10.1016/j.jnucmat.2004.04.129.

[8] M.J. Baldwin, R.P. Doerner, Helium induced nanoscopic morphology on tungsten under fusion relevant plasma conditions, Nucl. Fusion. 48 (2008) 35001. doi:10.1088/0029-5515/48/3/035001.

[9] M. Tokitani, S. Kajita, S. Masuzaki, Y. Hirahata, N. Ohno, T. Tanabe, Exfoliation of the tungsten fibreform nanostructure by unipolar arcing in the LHD divertor plasma, Nucl. Fusion. 51 (2011) 102001. doi:10.1088/0029-5515/51/10/102001.

[10] S.B. Gilliam, S.M. Gidcumb, N.R. Parikh, D.G. Forsythe, B.K. Patnaik, J.D. Hunn, L.L. Snead, G.P. Lamaze, Retention and surface blistering of helium irradiated tungsten as a first wall material, J. Nucl. Mater. 347 (2005) 289–297. doi:10.1016/j.jnucmat.2005.08.017.

[11] K. Wang, M.E. Bannister, F.W. Meyer, C.M. Parish, Effect of starting microstructure on helium plasma-materials interaction in tungsten, Acta Mater. 124 (2017) 556–567. doi:10.1016/j.actamat.2016.11.042.

[12] F. Hofmann, D. Nguyen-Manh, C.E. Beck, J.K. Eliason, M.R. Gilbert, a a Maznev, W. Liu, D.E.J. Armstrong, K. a Nelson, S.L. Dudarev, Lattice swelling and modulus change in a helium-implanted tungsten alloy: X-ray micro-diffraction, surface acoustic wave measurements, and multiscale modelling, Acta Mater. 89 (2015) 352–363.

[13] L. Pentecoste, P. Brault, A. Thomann, P. Desgardin, T. Lecas, T. Belhabib, Low energy and low fluence helium implantations in tungsten : Molecular dynamics simulations and experiments, J. Nucl. Mater. 470 (2016) 44–54. doi:10.1016/j.jnucmat.2015.12.017.

[14] L. Pentecoste, A. Thomann, A. Melhem, A. Caillard, S. Cuynet, T. Lecas, P. Brault, P. Desgardin, M. Barthe, Low flux and low energy helium ion implantation into tungsten using a dedicated plasma source, Nucl. Inst. Methods Phys. Res. B. 383 (2016) 38–46. doi:10.1016/j.nimb.2016.06.011.

[15] P.E. Lhuillier, T. Belhabib, P. Desgardin, B. Courtois, T. Sauvage, M.F. Barthe, A.L. Thomann, P. Brault, Y. Tessier, Helium retention and early stages of helium-vacancy complexes formation in low energy helium-implanted tungsten, J. Nucl. Mater. 433 (2013) 305–313. doi:10.1016/j.jnucmat.2012.09.001.

[16] T. Sauvage, H. Erramli, S. Guilbert, L. Vincent, M.F. Barthe, P. Desgardin, G. Blondiaux,

C. Corbel, J.P. Piron, F. Labohm, A. Van Veen, Profile measurements of helium implanted in UO2 sintered pellets by using the 3He(d, α)1H nuclear reaction analysis technique, J. Nucl. Mater. 327 (2004) 159–164. doi:10.1016/j.jnucmat.2004.02.002.

[17] F. Pászti, Microanalysis of He using charged particle accelerators Auger electron microscopy ERDwith foil filter ERDwith asymmetric coincidence ERDwith symmetric coincidence, Nucl. Instruments Andm. Phys. Res. B. 66 (1992) 83–106.

[18] J. Roth, B.M.U. Scherzer, R. Behrisch, P. Børgesen, The replacement of 3He implanted in Nb by subsequent 4He bombardment and vice versa, Nucl. Instruments Methods. 157 (1978) 75–81.

[19] R. Schulz, R. Behrisch, B.M.U. Scherzer, D and 3He trapping and mutual replacement in molybdenum, Nucl. Instruments Methods. 168 (1980) 295–299.

[20] W. Jaeger, J. Roth, He trapping and bubble formation in Ni, stainless steel 316 and amourphous alloys., Nucl. Instruments Methods. 182 (1980) 975–998. doi:10.1016/0029-554X(81)90831-4.

[21] A. Debelle, M.F. Barthe, T. Sauvage, First temperature stage evolution of irradiation-induced defects in tungsten studied by positron annihilation spectroscopy, J. Nucl. Mater. 376 (2008) 216–221. doi:10.1016/j.jnucmat.2008.03.002.

[22] P. Desgardin, L. Liszkay, M.-F. Barthe, L. Henry, J. Briaud, M. Saillard, L. Lepolotec, C. Corbel, G. Blondiaux, A. Colder, P. Marie, M. Levalois, Slow positron beam facility in Orléans, Mater. Sci. Forum. 363–365 (2001) 523–525. doi:10.4028/www.scientific.net/MSF.363-365.523.

[23] R. Krause-Rehberg, H.S. Leipner, Positron annihilation in semiconductors: defect studies, Springer Science & Business Media, 1999.

[24] V. Sabelová, V. Kršjak, J. Kuriplach, Y. Dai, V. Slugeň, Coincidence Doppler broadening study of Eurofer 97 irradiated in spallation environment, J. Nucl. Mater. 458 (2015) 350–354. doi:10.1016/j.jnucmat.2014.12.053.

[25] S.T. Picraux, F.L. Vook, Ion beam studies of H and He in metals, J. Nucl. Mater. 53 (1974) 246–251.

[26] S. Plimpton, Lammps Sandia, (1995). www.lammps.sandia.gov (accessed February 6, 2014).

[27] H.J.C. Berendsen, J.P.M. Postma, W.F. Van Gunsteren, A. DiNola, J.R. Haak, Molecular dynamics with coupling to an external bath, J. Chem. Phys. 81 (1984) 3684–3690. doi:10.1063/1.448118.

[28] J. Roth, E. Tsitrone, A. Loarte, T. Loarer, G. Counsell, R. Neu, V. Philipps, S. Brezinsek, M. Lehnen, P. Coad, C. Grisolia, K. Schmid, K. Krieger, A. Kallenbach, B. Lipschultz, R. Doerner, R. Causey, V. Alimov, W. Shu, O. Ogorodnikova, A. Kirschner, G. Federici, A. Kukushkin, Recent analysis of key plasma wall interactions issues for ITER, J. Nucl. Mater. 390–391 (2009) 1–9. doi:10.1016/j.jnucmat.2009.01.037.

[29] N. Juslin, B.D. Wirth, Interatomic potentials for simulation of He bubble formation in W,

J. Nucl. Mater. 432 (2013) 61–66. doi:10.1016/j.jnucmat.2012.07.023.

[30] D.E. Beck, A new interatomic potential function for helium, Mol. Phys. 14 (1968) 311–315. doi:10.1080/00268976800100381.

[31] W. Humphrey, A. Dalke, K. Schulten, VMD: Visual molecular dynamics, J. Mol. Graph. 14 (1996) 33–38. doi:10.1016/0263-7855(96)00018-5.

[32] G.J. Thomas, R. Bastasz, Direct evidence for spontaneous precipitation of helium in metals, J. Appl. Phys. 52 (1981) 6426–6428. doi:10.1063/1.328590.

[33] W.D. Wilson, C.L. Bisson, M.I. Baskes, Self-trapping of helium in metals, Phys. Rev. B. 24 (1981) 5616–5624. doi:10.1103/PhysRevB.24.5616.

[34] K.O.E. Henriksson, K. Nordlund, J. Keinonen, Molecular dynamics simulations of helium cluster formation in tungsten, Nucl. Instruments Methods Phys. Res. Sect. B Beam Interact. with Mater. Atoms. 244 (2006) 377–391. doi:10.1016/j.nimb.2005.10.020.

[35] L.M. Caspers, R.H.J. Pastenau, A. Van Veen, W.F.W.M. Van Heugten, Vacancies to Divacancies by Helium Trapping in Molybdenum, Phys. Status Solidi. 46 (1978) 541–546.

[36] M.S. Abd El Keriem, D.P. Van Der Werf, F. Pleiter, Trap mutation in He-doped ion-implanted tungsten, Hyperfine Interact. 79 (1993) 787–791.

[37] E. V Kornelsen, A.A. Van Gorkum, Enhanced penetration of low energy (25 eV-5000 eV) helium along the (100) channel in tungsten, Nucl. Instruments Methods Phys. Res. Sect. B Beam Interact. with Mater. Atoms. 170 (1980) 161–170.

[38] H.T. Lee, A.A. Haasz, J.W. Davis, R.G. Macaulay-Newcombe, D.G. Whyte, G.M. Wright, Hydrogen and helium trapping in tungsten under simultaneous irradiations, J. Nucl. Mater. 363–365 (2007) 898–903. doi:10.1016/j.jnucmat.2007.01.111.

[39] M.T. Robinson, The reflection of low energy helium atoms from tungsten surfaces, J. Nucl. Mater. 103–104 (1981) 525–530.

[40] F. Sefta, K.D. Hammond, N. Juslin, B.D. Wirth, Tungsten surface evolution by helium bubble nucleation, growth and rupture, Nucl. Fusion. 53 (2013) 73015. doi:10.1088/0029-5515/53/7/073015.

[41] M. Li, J. Cui, J. Wang, Q. Hou, Effect of cumulative helium bombardments on the surface and structural properties of tungsten, Nucl. Instruments Methods Phys. Res. Sect. B Beam Interact. with Mater. Atoms. 352 (2015) 92–95. doi:10.1016/j.nimb.2014.12.023.

[42] A.S. Soltan, R. Vassen, P. Jung, Migration and immobilization of hydrogen and helium in gold and tungsten at low temperatures, J. Appl. Phys. 70 (1991) 793–797.

[43] J. Amano, D.N. Seidman, Diffusivity of **3He atoms in perfect tungsten crystals., J. Appl. Phys. 56 (1984) 983–992. doi:10.1063/1.334039.

[44] F. Ferroni, X. Yi, K. Arakawa, S.P. Fitzgerald, P.D. Edmondson, S.G. Roberts, High temperature annealing of ion irradiated tungsten, Acta Mater. 90 (2015) 380–393. doi:10.1016/j.actamat.2015.01.067.

[45] D.R. Mason, X. Yi, M.A. Kirk, S.L. Dudarev, Elastic trapping of dislocation loops in cascades in ion-irradiated tungsten foils, (n.d.). doi:10.1088/0953-8984/26/37/375701.

[46] I. de Broglie, C.E. Beck, W. Liu, F. Hofmann, Temperature dependence of helium-implantation-induced lattice swelling in polycrystalline tungsten : X-ray micro-diffraction and Eigenstrain modelling, Scr. Mater. 107 (2015) 96–99. doi:10.1016/j.scriptamat.2015.05.029.

[47] G. Valles, M. Panizo-Laiz, C. Gonzalez, I. Martin-Bragado, R. Gonzalez-Arrabal, N. Gordillo, R. Iglesias, C.L. Guerrero, J.M. Perlado, A. Rivera, Influence of grain boundaries on the radiation-induced defects and hydrogen in nanostructured and coarse-grained tungsten, Acta Mater. 122 (2017) 277–286. doi:10.1016/j.actamat.2016.10.007.

[48] P.M.G. Nambissan, P. Sen, Positron annihilation studies on alpha irradiated tungsten, Solid State Commun. 71 (1989) 1165–1167.

[49] H.T. Lee, A.A. Haasz, J.W. Davis, R.G. Macaulay-Newcombe, Hydrogen and helium trapping in tungsten under single and sequential irradiations, J. Nucl. Mater. 360 (2007) 196–207. doi:10.1016/j.jnucmat.2006.09.013.

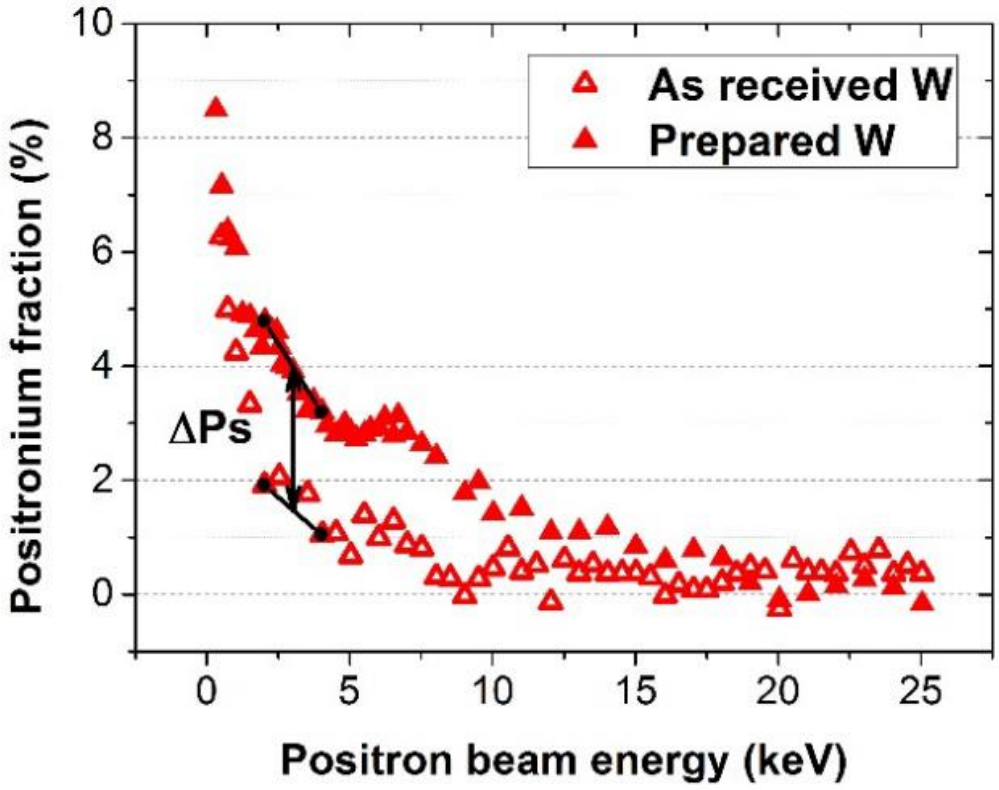

Figure 1: Fraction of emitted positronium for a tungsten as received (before preparation) and a prepared sample. Black lines locate the values with which the ΔPs/Ps factor is calculated.

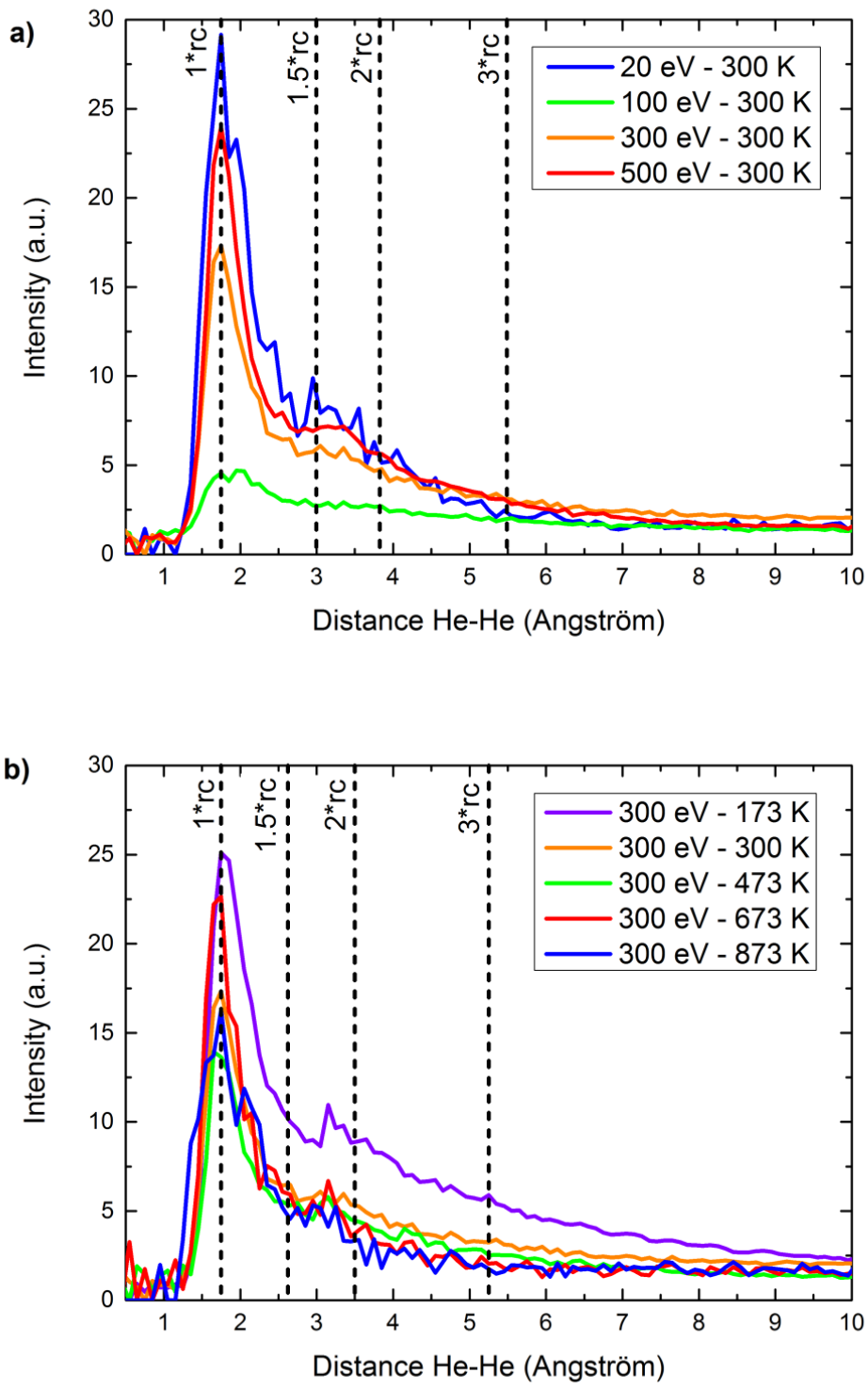

Figure 2 : a) RDFs of He atoms calculated for implantation simulations performed at 20, 100, 300 and 500 eV and a temperature of 300 K. b) RDFs of He atoms calculated for implantation. simulations performed at 300 eV and temperatures of 173, 300, 473, 673 and 873 K. Each RDF is calculated at the end of the simulation.

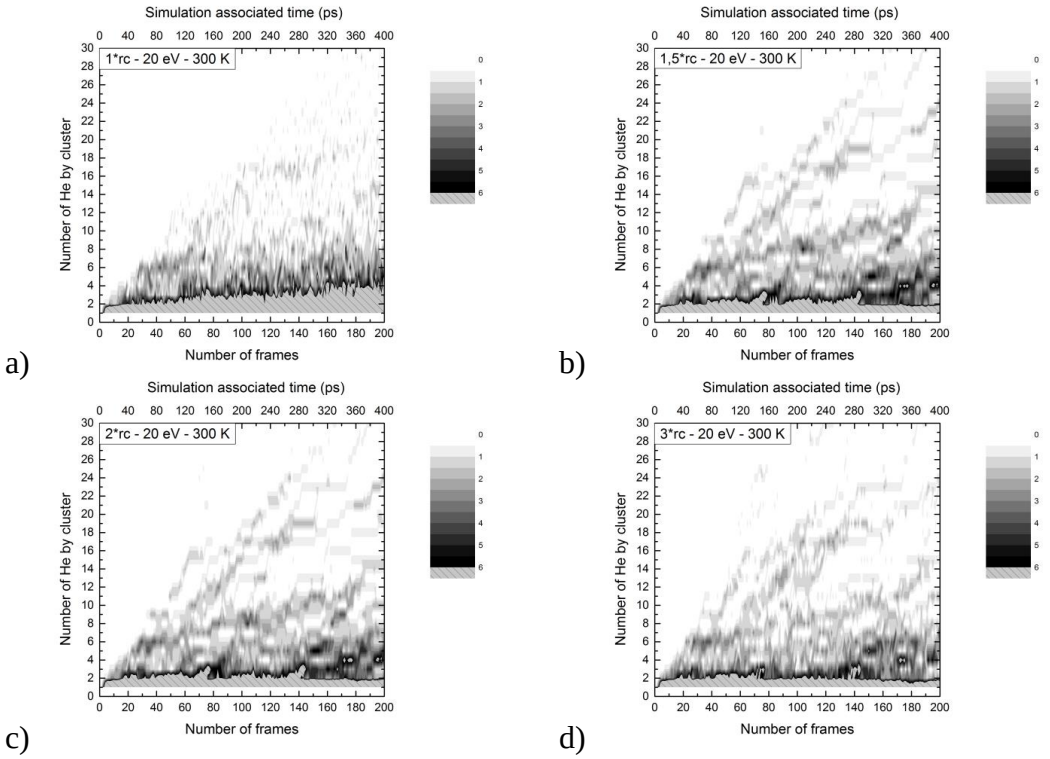

Figure 3: Histograms presenting the number of He atoms by cluster as a function of the frame or time step of the simulation. The color scale indicates the number of Hen clusters containing the number n of He atoms. The rc in each graphs is 1.75 Å (a), 2.625 Å (b), 3.5 Å (c) and 5.25 Å (d).

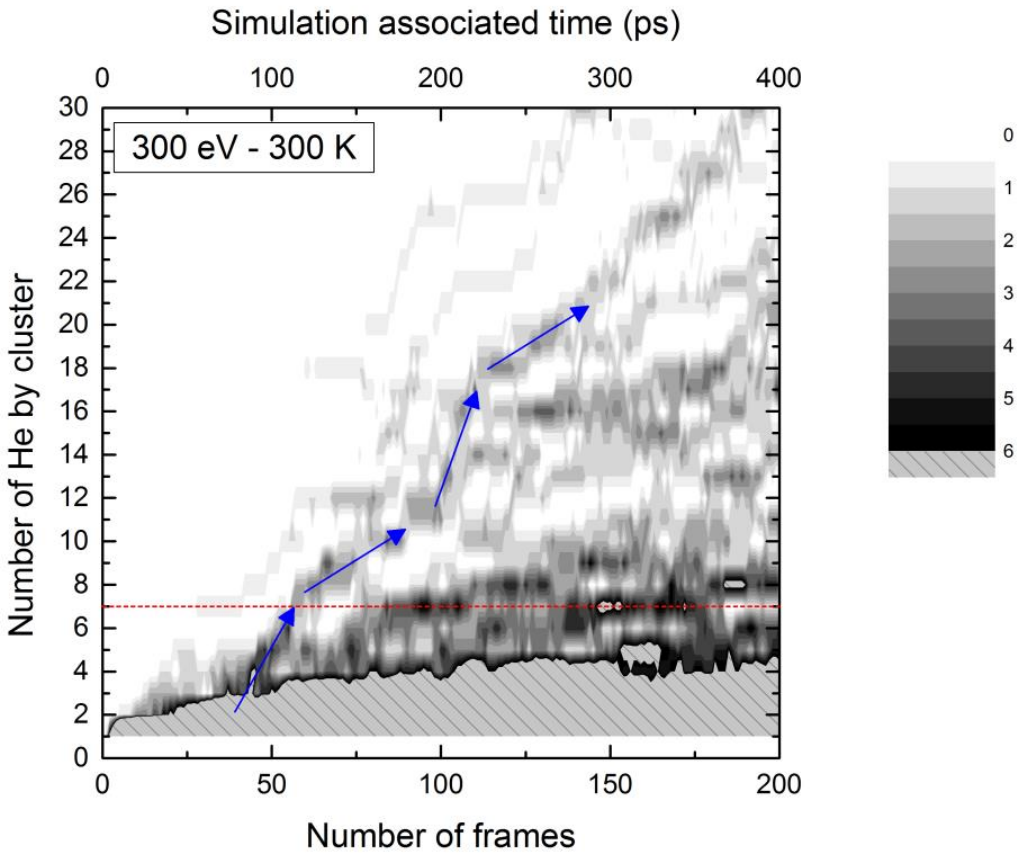

Figure 4: Number of He in the cluster as a function of the frame or time step. The color scale indicates the number of clusters present in the W lattice. The implantation conditions for this histogram are 300 eV and 300 K. The red dotted line corresponds to the levelling of the plot for a number of He per cluster of 7. The blue arrows follow the growth of some representative clusters.

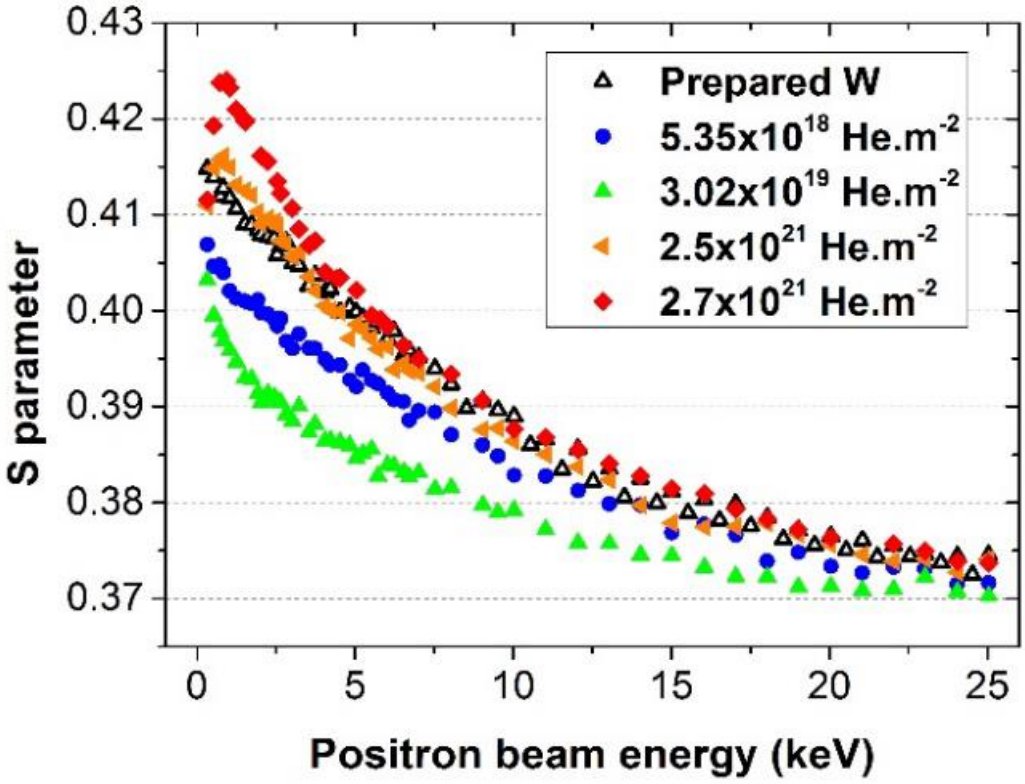

Figure 5: Evolution of the S parameter with the positron kinetic energy for tungsten samples implanted at various impinging fluences. The curve for a tungsten sample before implantation (prepared W) is also provided.

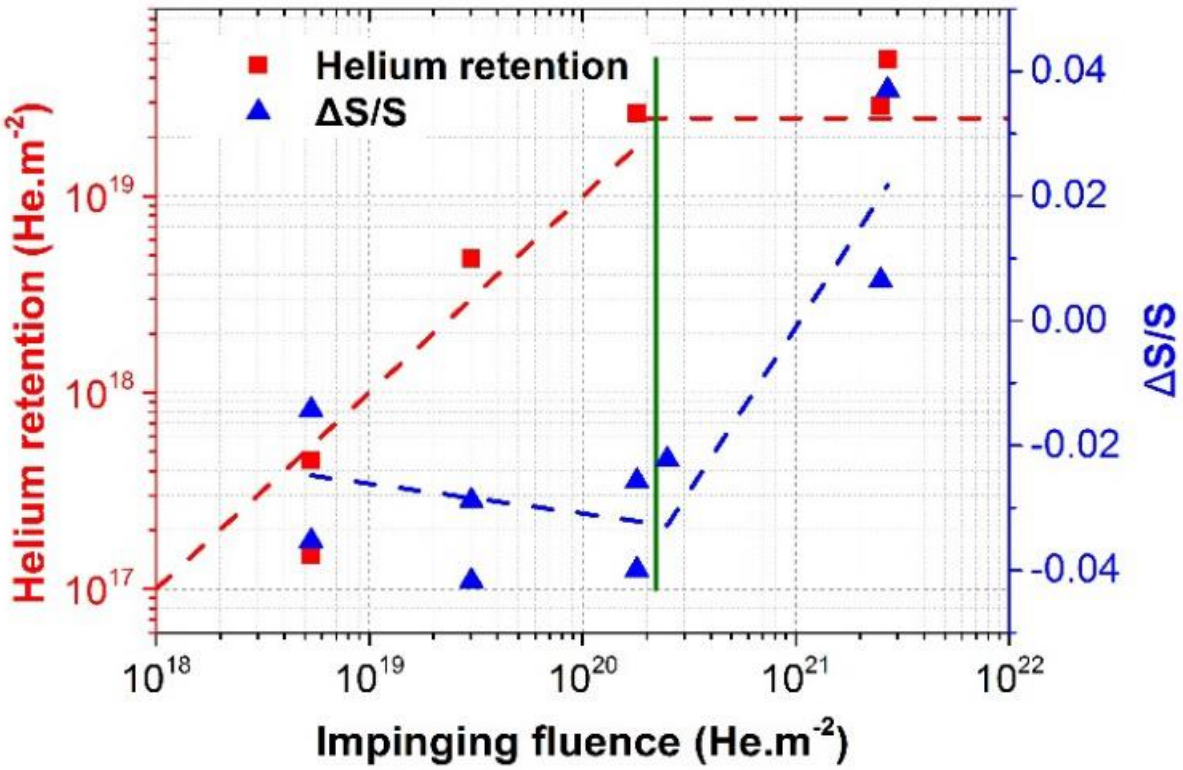

Figure 6: Evolution of the retention (measured by NRA, red squares) and of the deviation of the S parameter from the initial state (ΔS/S) determined by DB-PAS as function of the impinging fluence (blue triangles).

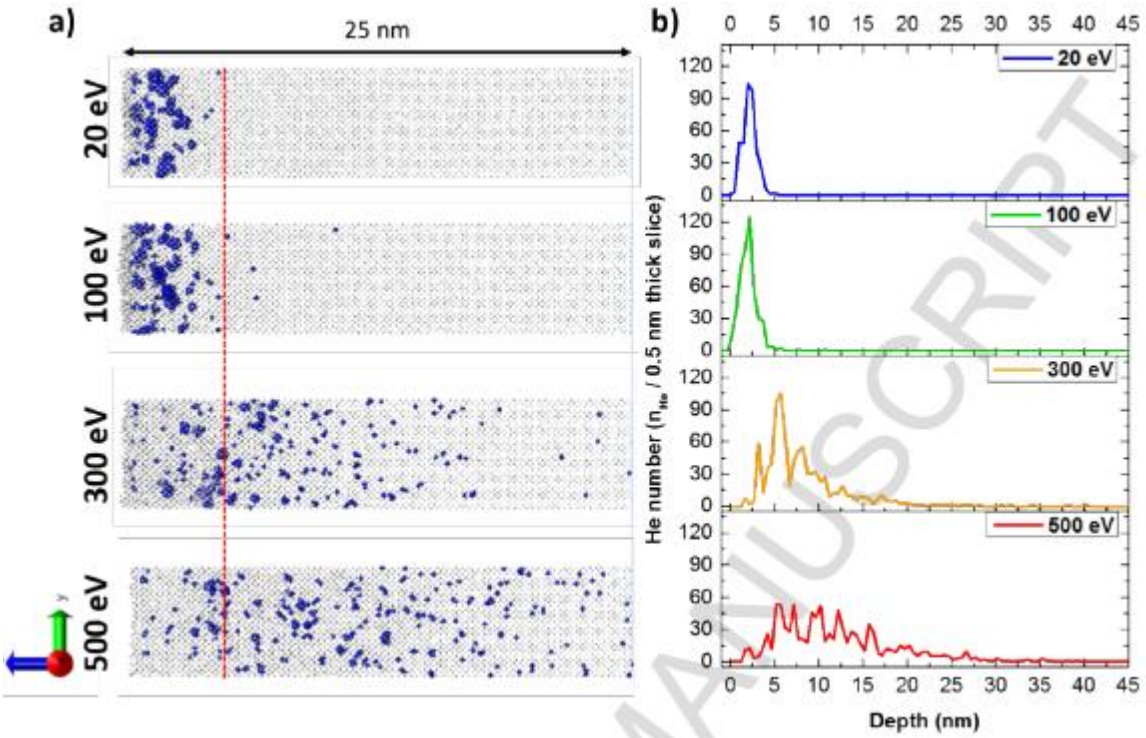

Figure 7: Results of MD simulation of He implantation in tungsten at room temperature depending on the kinetic energy of the incident helium ions for $1.3x10^{19}$ $He.m^{-2}$ retention. a) Snapshots of the implantation simulations. The surface of the W is located at the left side of the images. The gray dots stand for the W atoms and the blue ones for the He atoms. The red dashed line stands for the frontier between the depth at which defects are (on the right) and are not (on the left) detected by DB-PAS. b) He concentration profiles aligned with corresponding snapshots.

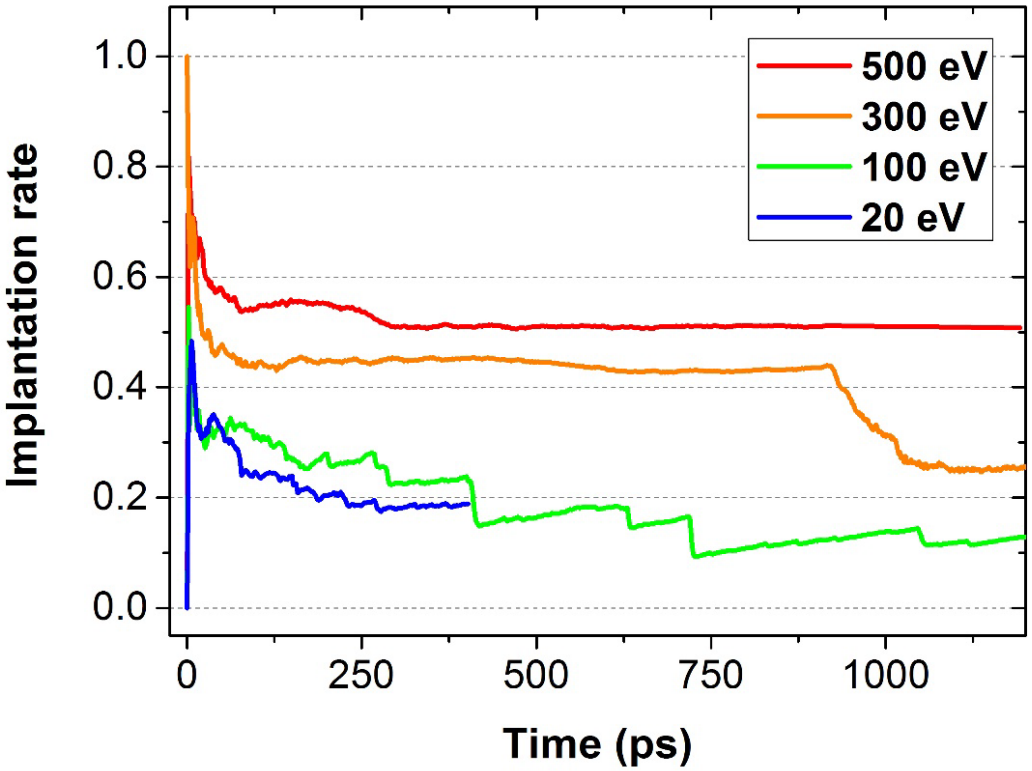

Figure 8: Time dependence of the He retention rate for various kinetic energies of the incident He atoms for MD simulated implantations at room temperature.

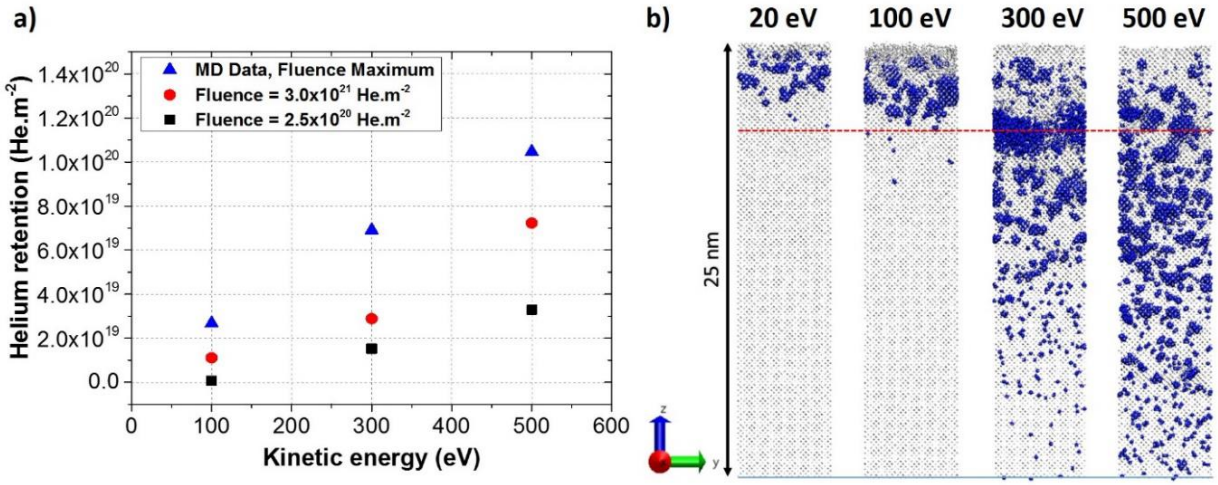

Figure 9: a) Evolution with the He ion kinetic energy of He retention as measured by NRA at high ($3.1x10^{21}$ $He.m^{-2}$) and low ($2.5x10^{20}$ $He.m^{-2}$) impinging fluences and as calculated from MD simulation at the maximum simulated impinging fluences for 20, 100 and 500 eV and at the saturation step for 300 eV; b) corresponding snapshots. The red dashed line stands for the frontier between the depth at which defects are (below the line) and are not (above the line) detected by DB-PAS. Experiments and simulations were performed at room temperature

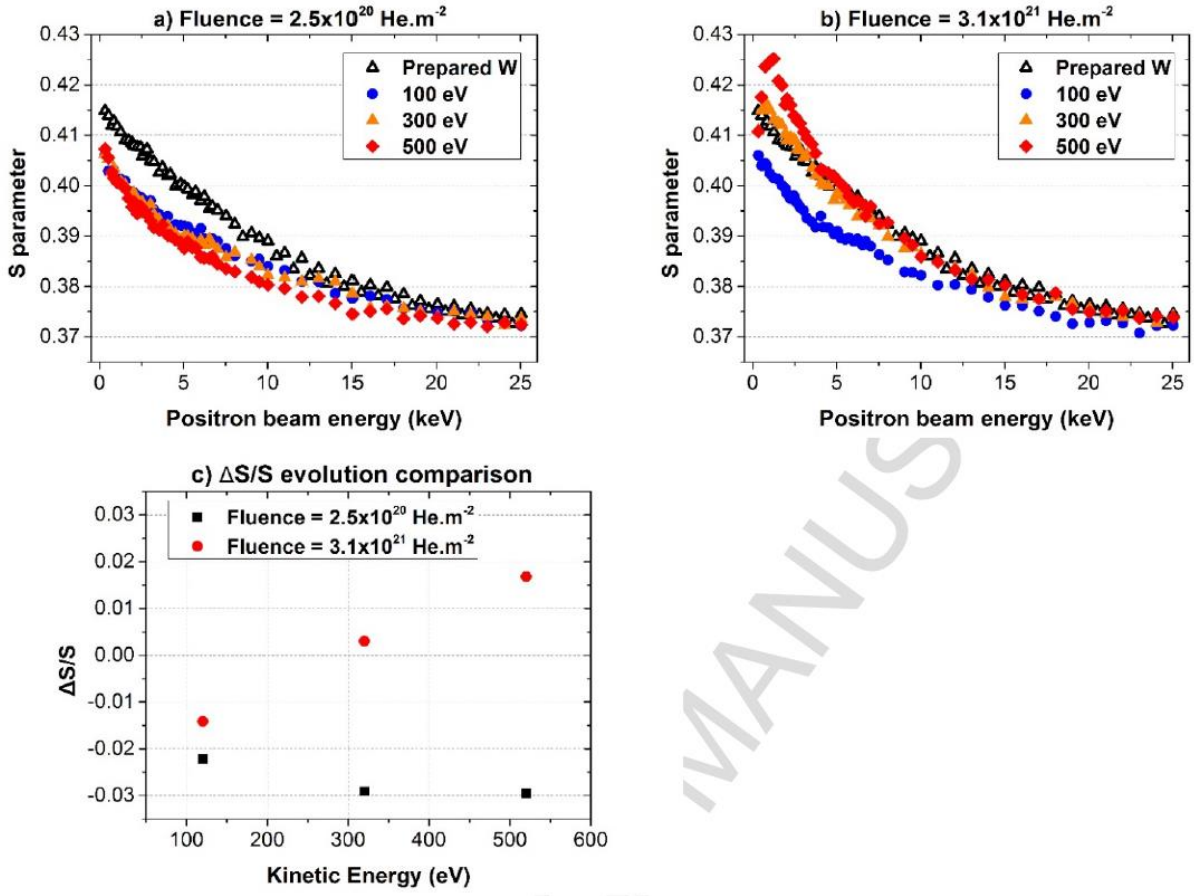

Figure 10: Evolution of the S parameter with the positron kinetic energy for various kinetic energies of the incident helium ions for two impinging fluences and at room temperature (a and b). The corresponding evolution of the ΔS/S parameter is also given (c).

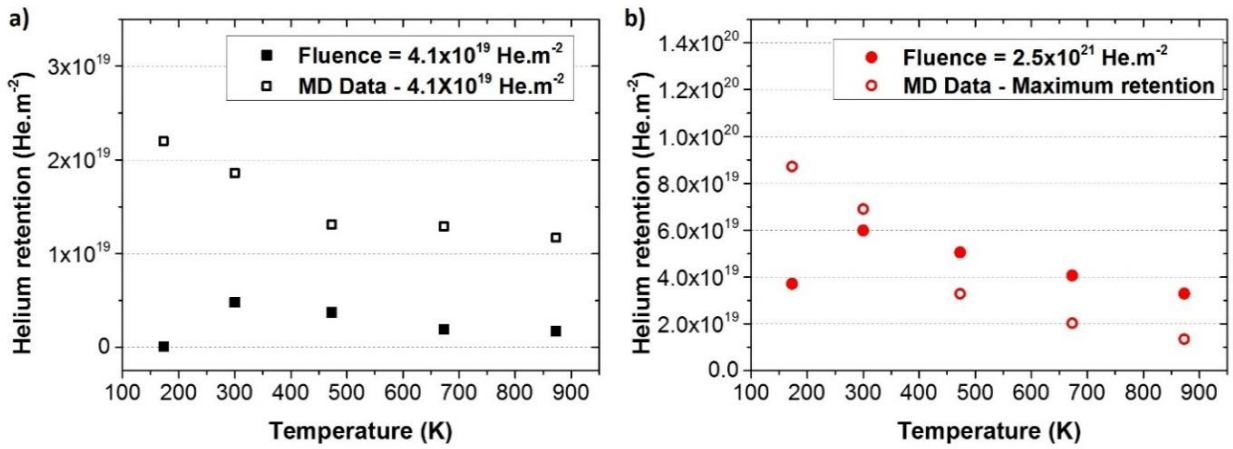

Figure 11: Evolution of the He retention as measured by NRA as a function of the substrate temperature during the implantation at low (a : $4.1x10^{19}$ $He.m^{-2}$) and high (b : $2.5x10^{21}$ $He.m^{-2}$), impinging fluences. MD Calculated implanted fluences are presented for equivalent low impinging fluence $4.1x10^{19}$ $He.m^{-2}$ and for high impinging fluence, the implanted fluence is given at the step just before the substrate rupture. The He^{+} ion kinetic energy is 300 eV.

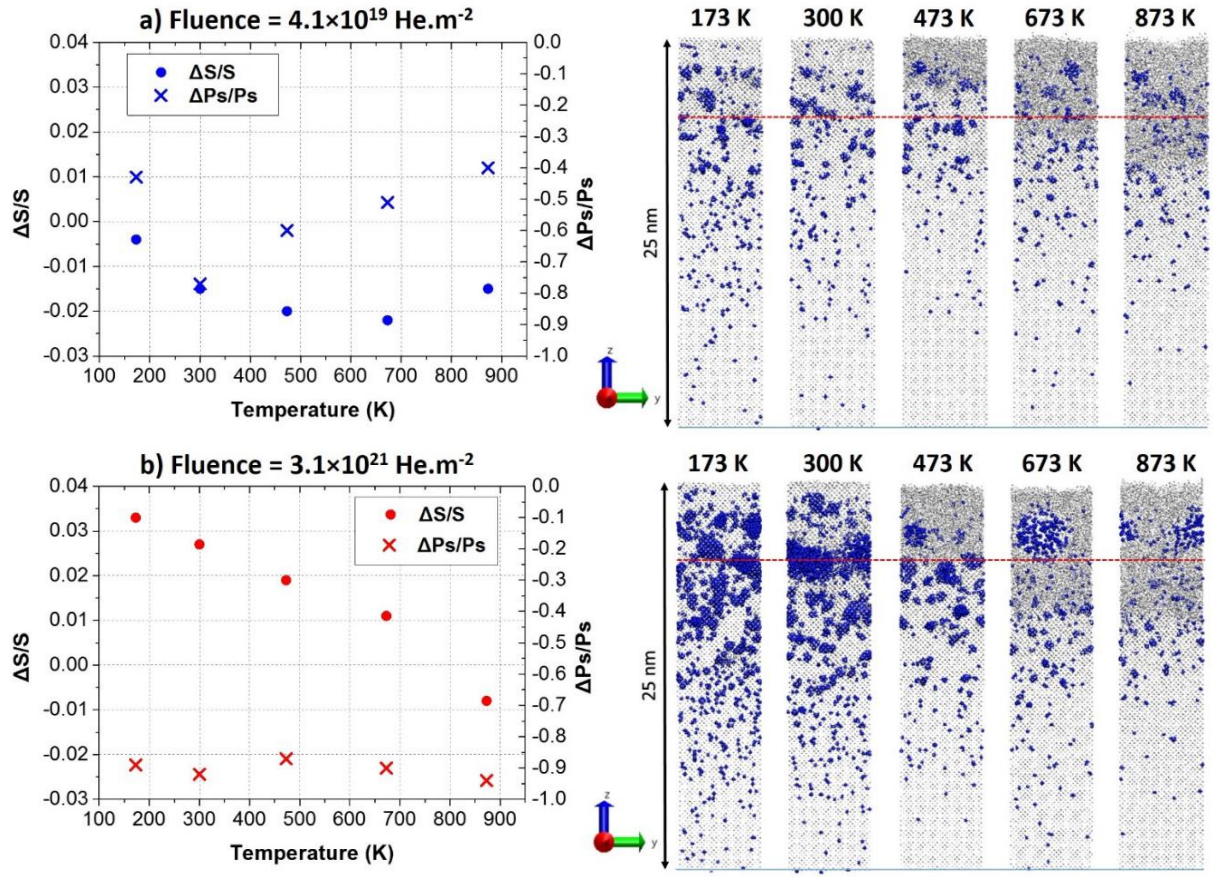

Figure 12: Deviations of S and Ps from the initial state for low (a) and high (b) impinging fluences and corresponding MD snapshots depending on the substrate temperature at 300 eV He^+ kinetic energy. For the high fluence case, the snapshots illustrate the moment at which the saturation is reached for each simulation.

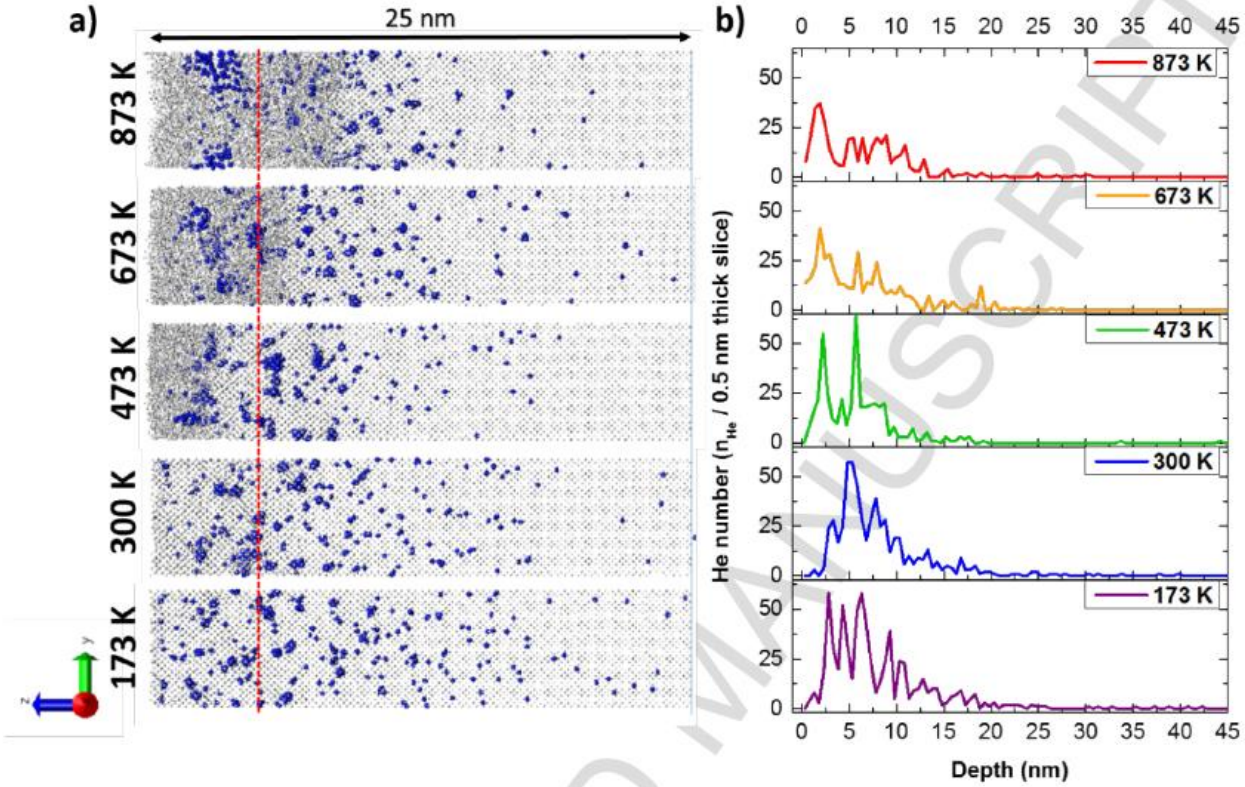

Figure 13: Results of MD simulation of He implantation in W at 300 eV depending on the temperature of the tungsten substrate for a retention of 1.4×10^{19} He.m^{-2}. a) snapshots; b) He concentration profiles.

Table 1: a) Number of He necessary to form a Hen-V cluster for various incident kinetic energies of the He atoms. b) Number of He necessary to form a Hen-V cluster for various W substrate temperatures.

a) He kinetic energy (eV)	20	100	300	500
$n_{He/cluster}$	6	8	7	7

b) W substrate temperature (K)	173	300	473	673	873
$n_{He/cluster}$	6-8	7	5-7	5-7	-